

## Polaron-induced anti-Stokes photoluminescence under selective excitation in diluted magnetic semiconductors

Takanori Okada<sup>1</sup> and Tadashi Itoh<sup>2</sup><sup>1</sup>*Pioneering Research Unit for Next Generation, Kyoto University, Kyoto 615-8245, Japan*<sup>2</sup>*Institute for NanoScience Design, Osaka University, Osaka 560-8531, Japan*

(Received 6 June 2010; revised manuscript received 25 March 2011; published 29 April 2011)

Anti-Stokes photoluminescence is observed under selective excitation in a bulk sample of the diluted magnetic semiconductor  $\text{Cd}_{1-x}\text{Mn}_x\text{Te}$  with  $x = 0.2$ . The anti-Stokes photoluminescence is induced by a two-step optical-absorption process that creates excitons via an alloy potential state and an impurity center. Both localized exciton magnetic polarons bound to the fluctuating alloy potential and exciton magnetic polarons bound to neutral acceptors participate in forming intermediate states with long lifetimes that cooperatively contribute to the anti-Stokes photoluminescence. The reabsorption of the anti-Stokes photoluminescence is also examined by considering the role of bound magnetic polarons. The localized  $\text{Mn}^{2+}$  spin ordering in magnetic polarons bound to the impurity center largely contributes in reducing reabsorption.

DOI: [10.1103/PhysRevB.83.155211](https://doi.org/10.1103/PhysRevB.83.155211)

PACS number(s): 75.50.Pp, 78.20.Ls, 78.55.Et, 78.60.-b

### I. INTRODUCTION

Diluted magnetic semiconductors (DMSs), which are compound semiconductors doped with magnetic ions, are currently being widely studied both theoretically and experimentally and have attracted attention in the field of spintronics. The physical properties of DMSs involve a combination of semiconductor mixed-crystal effects and magnetism associated with the unpaired spins.<sup>1,2</sup> According to the virtual crystal approximation, the alloy potential in these mixed compounds should fluctuate, leading to the intrinsic localization of photoexcited excitons.<sup>3</sup> The most important physical properties are based on strong exchange interactions between the spins of photoexcited electrons or holes and the spins of the local magnetic ions. These exchange interactions can result in the effective  $g$  factors of DMSs being enhanced by up to two orders of magnitude with respect to those of nonmagnetic semiconductors, which leads to peculiar magneto-optical effects such as giant Zeeman splitting of the valence and conduction bands, giant Faraday rotation,<sup>4</sup> the formation of magnetic polarons,<sup>5</sup> and photoinduced magnetization.<sup>6</sup> Localization of the excitons or carriers induces the alignment of magnetic spins inside their Bohr radius, thereby resulting in the formation of either a self-trapped localized exciton magnetic polaron (LMP) bound to an alloy potential fluctuation, or of a so-called bound exciton magnetic polaron (BMP) involving a magnetic polaron bound to a charged impurity.

One of the most interesting phenomena exhibited by DMSs is ferromagnetism,<sup>7</sup> which has been attributed to a large effective magnetic field (also referred to as an exchange field) arising from ferromagnetic interactions between BMPs, to their percolation,<sup>8,9</sup> or to ferromagnetic correlations mediated by holes.<sup>10</sup> Magnetization can be induced in DMSs by optical spin pumping with circularly polarized radiation,<sup>6</sup> potentially giving rise to photoinduced phase transitions between ferromagnetic and paramagnetic states, even in bulk alloys.

In order to realize the kind of phenomena mentioned above, wide-gap semiconductor-based DMSs such as  $\text{Cd}_{1-x}\text{Mn}_x\text{Te}$  are good candidates because their electric and magnetic properties are well enough studied to be exploited for practical

uses, which include optomagnetic devices utilizing spin manipulation as well as optoelectronic effects in the visible frequency region. Ferromagnetic properties can be realized in quantum well structures in this material by  $p$ -type modulation doping.<sup>11,12</sup>

The photoluminescence (PL) of  $\text{Cd}_{1-x}\text{Mn}_x\text{Te}$  is ascribed to the exciton magnetic polarons and has been well studied.<sup>5</sup> The dominant exciton magnetic polaron PL lines are the so-called  $L_1$  and  $L_2$  lines, which at low temperature arise from exciton magnetic polarons bound to a neutral acceptor ( $A^0XBMP$ ) and from self-trapped LMPs, respectively. Below 4 K the  $L_1$  peak has been observed for Mn compositions  $0 < x < 0.36$ .<sup>13,14</sup> The existence of the  $L_2$  peak has been reported for  $0.05 < x < 0.4$ .<sup>13</sup> The  $L_1$  line exhibits  $\sigma^-$  circular polarization with Faraday geometry<sup>15</sup> whereas the  $L_2$  line exhibits  $\sigma^+$  circular polarization.<sup>1</sup> The PL provides information on the magnetic properties of  $\text{Cd}_{1-x}\text{Mn}_x\text{Te}$  via the excitonic states. In particular, the anti-Stokes PL (sometimes referred to as up-conversion PL), which is located on the higher energy side of the excitation energy, is interesting from the point of view of fundamental microscopic examinations of the state (mode) of phonons, electrons, and spins, and of their interactions with photons. This is because, although the quantum efficiency of the anti-Stokes PL is usually very small, it contains a variety of information on complex exciton transfer in the energy levels of DMS bulk alloys, nanoparticles, and heterostructures.<sup>16-18</sup> Furthermore, anti-Stokes PL is advantageous for measuring the tiny localized magnetic or electric perturbations associated with the exciton magnetic polarons or excitons. This is because the excitation light penetrates deep into the bulk alloy sample and anti-Stokes PL is reabsorbed as it propagates back to the surface, which implies that the interaction length of the excitation light with excitonic matter is greater than in standard absorption measurements in thin samples. The anti-Stokes PL in semiconductors is also of practical significance; for example, optical data recording and anti-Stokes fluorescence cooling in macroscopic systems has been reported.<sup>19</sup>

In this paper, we report on the observation of anti-Stokes PL in bulk  $\text{Cd}_{0.8}\text{Mn}_{0.2}\text{Te}$  using site-selective spectroscopy.

We discuss its mechanism and characteristics including the relationship to Stokes PL, which is located on the lower energy side of the excitation energy. We also study the reabsorption of anti-Stokes PL by considering the effect of photoinduced localized  $\text{Mn}^{2+}$  spin ordering within  $A^0\text{XBMPs}$ . Moreover, we demonstrate that PL due to the recombination of LMPs appears in the vicinity of PL arising from the recombination of the  $A^0\text{XBMPs}$ .<sup>15</sup>

## II. EXPERIMENT

We investigated a bulk  $\text{Cd}_{1-x}\text{Mn}_x\text{Te}$  sample with  $x = 0.2$  grown using the Bridgman method. The sample was mounted inside a cryostat equipped with a superconducting-coil magnet able to generate magnetic fields up to 7.5 T parallel to the wave vector of the light source (Faraday geometry). All measurements were conducted at a temperature of 4.5 K, controlled using a continuous flow of liquid helium and a heater.  $\text{Cd}_{0.8}\text{Mn}_{0.2}\text{Te}$  is paramagnetic at temperatures above  $\sim 2\text{ K}$ <sup>20</sup> in the absence of optical excitation.

The stationary PL characteristics were measured as a function of excitation energy, excitation power, and applied magnetic field. The light source used for selective excitation ( $\lambda_{\text{ex}} = 600\text{--}690\text{ nm}$ ) consisted of a dye laser (with a DCM laser dye solution) pumped by all the lines of an argon-ion laser. The light source was spectrally resolved using a monochromator. For band-to-band excitation, the second harmonic of a Nd:YVO<sub>4</sub> laser (532 nm) was also used as an excitation source. The light source, the spot size of which focused on the sample was 0.5 mm, was placed perpendicular to the sample surface. For measurements using a circularly polarized excitation source, a polarizer and a quarter-wave plate were placed in front of the sample. The backward PL from the sample was passed through a quarter-wave plate and a polarizer in order to separate the  $\sigma^+$  and  $\sigma^-$  circular polarization. The PL was recorded using a charge-coupled device (CCD) array cooled to liquid-nitrogen temperature, after first being passed through a triple spectrometer with a focal length of 64 cm and equipped with a grating of 1800 grooves/mm in order to suppress scattered laser light with energies close to that of the PL. The spectral resolution was better than 0.1 nm (0.3 meV). A tungsten lamp was used to correct the PL intensity, because the spectra are modified by the inhomogeneous sensitivity of the CCD sensor array and the grating. All lenses in the optical setup were achromatic.

## III. RESULTS AND DISCUSSION

### A. Characteristics of anti-Stokes photoluminescence

Figure 1(a) shows typical PL spectra of our bulk  $\text{Cd}_{0.8}\text{Mn}_{0.2}\text{Te}$  sample at various excitation energies and zero magnetic field. The (Stokes) PL in the top spectrum was measured under band-to-band excitation. With decreasing excitation energy, the maximum of the Stokes PL peak is shifted to slightly higher energy, as presented in Fig. 1(b); the intensity of this peak also increases initially, reaching a maximum value at an excitation energy of 1.925 eV that is 1.9 times greater than the Stokes PL intensity under band-to-band excitation, as shown in Fig. 1(c). The peak intensity then falls rapidly as the excitation energy is decreased further,

and the position of the peak maximum also decreases with a constant Stokes shift of  $\Delta E = 15\text{ meV}$  [Fig. 1(b)], which corresponds to the localization energy associated with the formation of exciton magnetic polarons.<sup>21</sup> The greatest rate of decrease of the Stokes PL intensity is observed below the excitation energy of 1.905 eV [Fig. 1(c)], which is close to the energy of the (Stokes) PL peak maximum under band-to-band excitation [top spectrum in Fig. 1(a)]. The three extremely weak peaks evident below the PL maximum at an excitation energy of 1.89 eV in Fig. 1(a) can be assigned to MnTe LO<sub>1</sub> (24.49 meV), CdTe LO<sub>2</sub> (20.25 meV), and CdTe TO<sub>2</sub> (17.68 meV) Raman Stokes lines.<sup>2</sup> Below the excitation energy at which the Stokes PL intensity decreases at the greatest rate (1.905 eV), an anti-Stokes PL feature appears as shown in Figs. 1(a) and 1(b). As presented in the inset of Fig. 1(d), the anti-Stokes PL is clearly observed at excitation energies higher than 1.87 eV, below which the intensity is small and gradually decreases further. We note that the anti-Stokes PL is not due to laser-scattered light, because the intensity on the low-energy side of the peak is already decreasing before the cutoff point, as shown in the inset of Fig. 1(d).

### B. Mechanism of generation of anti-Stokes photoluminescence

The anti-Stokes PL spectra show a characteristic dependence on the excitation power (Fig. 2). Stokes and anti-Stokes PL are observed at 1.875 and 1.905 eV, respectively, when the excitation energy is 1.891 eV (Fig. 2, inset). A double logarithmic plot of the integrated intensity of the anti-Stokes PL peak versus excitation power reveals two linear regimes. At low excitation power the slope is 2, corresponding to a quadratic dependence of the anti-Stokes intensity on excitation power, whereas the slope is linear when the excitation power is greater than 3 mW/cm<sup>2</sup>. This linear dependence is observed over the entire power regime in the Stokes PL spectra. From general arguments, the microscopic mechanisms that give rise to anti-Stokes PL are Auger recombination,<sup>22</sup> thermal activation by the absorption of phonons, and the contribution of two or more photons to the optical excitation process. Because the anti-Stokes PL diminishes rapidly with increasing temperature and completely disappears at temperatures higher than 20 K (the corresponding thermal energy here is  $k_{\text{B}}T \approx 1.8\text{ meV}$  where  $k_{\text{B}}$  is the Boltzmann constant), thermal processes can be excluded. Anti-Stokes PL due to both Auger recombination and two-photon or multiple-photon absorption processes can also be ruled out because a quadratic or higher-order dependence on excitation density would then be followed for the entire power regime. Moreover, these are well-known optical phenomena in nonlinear processes, which require high excitation power. The Auger process is also inefficient in the bulk alloy at low temperatures due to the condition of momentum conservation.

Therefore we propose that the dominant mechanism of the anti-Stokes PL involves the combination of a two-step absorption process<sup>16,18</sup> with cooperative excitation.<sup>17</sup> The appearance of the anti-Stokes PL at temperatures lower than 20 K, at which the exciton magnetic polarons exist,<sup>23</sup> implies that the latter play an essential role in this mechanism. In the following discussion, illustrated schematically in Fig. 3, we explain that the anti-Stokes PL can be ascribed to a two-step

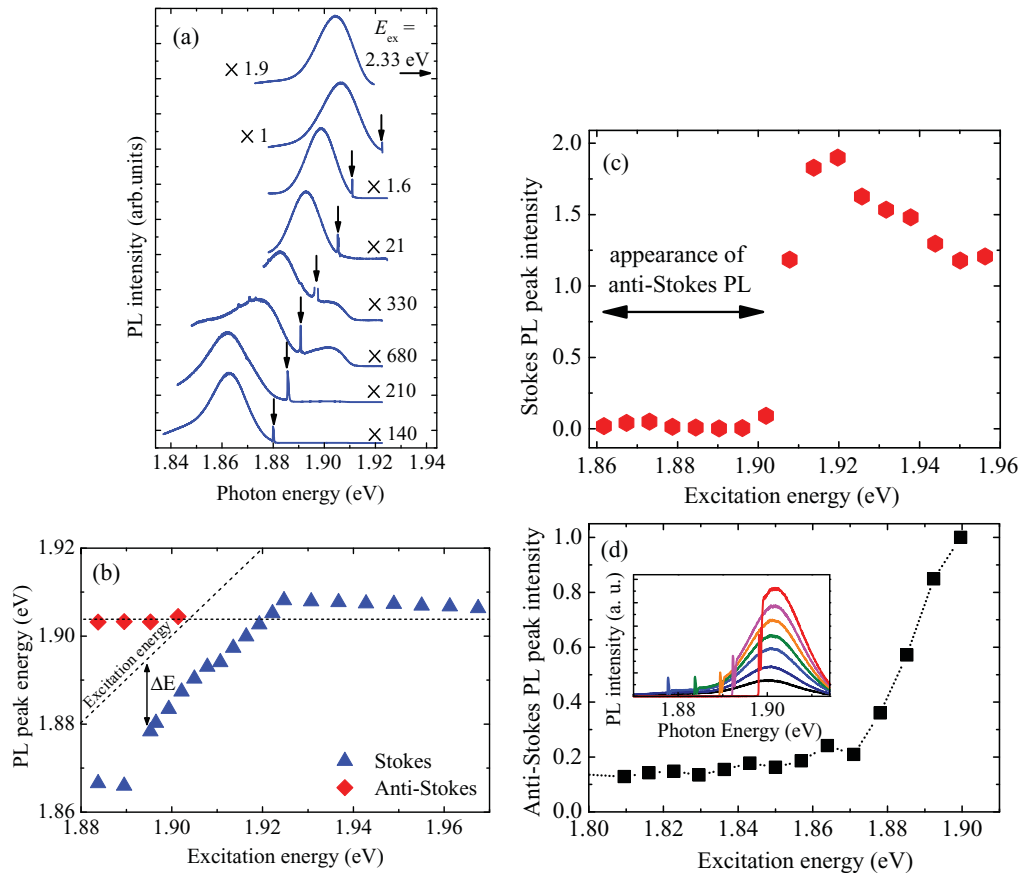


FIG. 1. (Color online) (a) Stationary PL spectra of excitons in bulk  $\text{Cd}_{0.8}\text{Mn}_{0.2}\text{Te}$  under selective excitation at different energies and zero magnetic field. The peak intensities are normalized to that of the Stokes PL peak (top spectrum). The excitation power and temperature were fixed at  $400 \text{ mW/cm}^2$  and  $4.5 \text{ K}$ . (b) Position of PL peak as a function of excitation energy.  $\Delta E$  indicates the localization energy due to the formation of exciton magnetic polarons. (c) Dependence of Stokes PL peak intensity on excitation energy. The peak intensities are normalized to the Stokes PL intensity under band-to-band excitation. (d) Dependence of anti-Stokes PL peak intensity on excitation energy. The peak intensities are normalized to that measured at an excitation energy of  $1.9 \text{ eV}$ . The inset shows the evolution of anti-Stokes PL spectra at various excitation energies.

absorption process involving both LMP states and  $A^0\text{XBMP}$  states. First, electron-hole pairs are created that relax to form localized excitons, which are strongly localized by the alloy potential fluctuation. These excitons then relax further to form LMPs (hereafter referred to as the first localized state), which are lower in energy than the equilibrium distribution center of the exciton magnetic polarons. A Stokes  $L_2$  line, located below the excitation energy, is generated when the LMPs dissociate. On relaxation, some of the electron-hole pairs also couple with the neutral acceptor bound states to form  $A^0\text{XBMPs}$  (hereafter referred to as the second localized state), which are located at slightly lower energy than the first localized state. Some  $A^0\text{XBMPs}$  might then absorb a second photon associated with the Stokes  $L_2$  line. Other  $A^0\text{XBMPs}$  dissociate to generate a Stokes  $L_1$  line. Because the number of acceptors available is limited, the second localized state is easily saturated with increasing excitation power. The capture of a second photon by  $A^0\text{XBMPs}$  in the second localized state leads to the creation of electron-hole pairs with energies higher than the alloy potential fluctuation, and results in the formation of further LMPs and  $A^0\text{XBMPs}$  after relaxation to states that are lower in energy than the mobility edge of the alloy potential fluctuation. The

radiative recombination of these LMPs and  $A^0\text{XBMPs}$ , which have higher energies than the initial excitation photon, then gives rise to the anti-Stokes PL. We note that the coupling between the  $A^0\text{XBMPs}$  and the photons associated with the Stokes  $L_2$  line is optically allowed, because the Stokes  $L_2$  line from excitons with total angular momentum  $J = 1$  in LMPs resonantly excites the excitons with  $J = -1$  in  $A^0\text{XBMPs}$ . We have confirmed that the  $L_1$  and  $L_2$  lines appear in both Stokes and anti-Stokes PL. Here, we assume that the relaxation time to the first and second localized states is short compared to the lifetime of the localized excitons.

We note that two other two-step absorption processes can also be considered regarding the generation of anti-Stokes PL; it is possible that both the first and second localized states could be comprised of either  $A^0\text{XBMPs}$  or LMPs. In the former case, both types of  $A^0\text{XBMP}$  localized states would saturate with increasing excitation power, in contrast to the linear dependence of the anti-Stokes PL intensity on excitation power shown in Fig. 2. Regarding the latter possibility, we observed that the intensity of the Stokes  $L_2$  line is linearly dependent on excitation power; this holds even when the  $\text{Mn}^{2+}$  content is low and the intensity is correspondingly

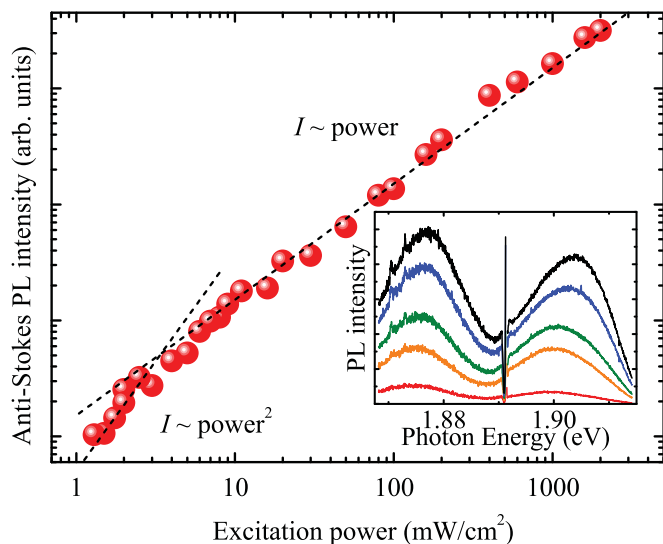


FIG. 2. (Color online) Double logarithmic plot of the dependence of integrated anti-Stokes PL intensity on excitation power at an excitation energy of 1.891 eV. The dashed lines indicate quadratic and linear fits to the experimental data. The temperature was fixed at 4.5 K and the excitation power was varied from 1.34 to 2000 mW/cm<sup>2</sup>. The inset shows PL spectral features at selected values of excitation power.

weak, which is inconsistent with the linear trend in the anti-Stokes PL intensity in Fig. 2. Therefore these two alternative processes cannot be dominant. We thus conclude that the intermediate states involved in the generation of anti-Stokes PL are comprised of LMPs as the first localized state and A<sup>0</sup>XBMPs as the second localized state. This is consistent with a scenario where the excitonic energy distribution due to the alloy potential fluctuation causes a gradual increase in anti-Stokes PL intensity with excitation energy above 1.87 eV, as apparent in Fig. 1(d). We also conclude that a certain proportion of the Stokes PL is absorbed, exciting some of the electron-hole pairs in A<sup>0</sup>XBMPs to energies higher than the alloy potential fluctuation, a process known as “photon recycling.” This explains why the anti-Stokes PL appears at excitation energies where the intensity of the Stokes PL line drastically decreases, as shown in Fig. 1(c).

We will now use these ideas to construct a quantitative model. We assume all the created excitons to form localized excitons or A<sup>0</sup>Xs. The simultaneous rate equations describing the localized exciton (subsequently LMP) density  $n_L$ , the A<sup>0</sup>X (subsequently A<sup>0</sup>XBMP) density  $n_{A_0X}$ , and the localized exciton (subsequently magnetic polaron) density contributing to both the anti-Stokes L<sub>1</sub> and L<sub>2</sub> lines  $n_{AS}$  are given by

$$\frac{dn_L}{dt} = pn_E - \frac{n_L}{\tau_L} - C_{L-A_0}n_L(N_{A_0} - n_{A_0X}), \quad (1)$$

$$\frac{dn_{A_0X}}{dt} = (1-p)C_{E-A_0}n_E(N_{A_0} - n_{A_0X}) + C_{L-A_0}n_L \times (N_{A_0} - n_{A_0X}) - \frac{n_{A_0X}}{\tau_{A_0X}} - Wn_Ln_{A_0X}, \quad (2)$$

$$\frac{dn_{AS}}{dt} = -\frac{n_{AS}}{\tau_{AS}} + Wn_Ln_{A_0X}, \quad (3)$$

where  $n_E = q\alpha I_{ex} \exp(-\alpha x_E)/h\nu_{ex}$  represents the exciton generation rate per unit volume per unit time (cm<sup>-3</sup> sec<sup>-1</sup>),  $q$

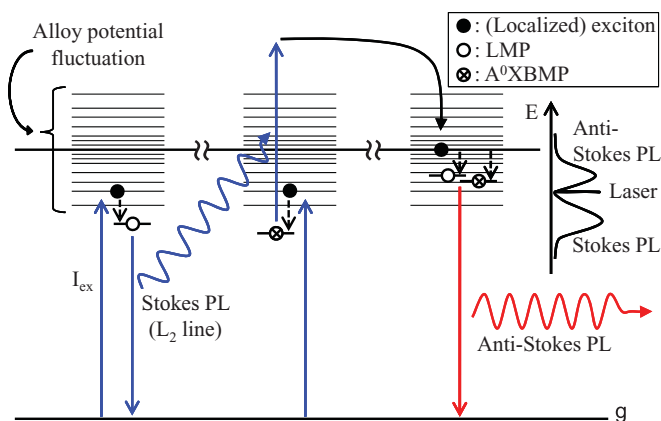


FIG. 3. (Color online) Schematic illustration of excitation processes giving rise to anti-Stokes PL. The first localized state in the intermediate state consists of LMPs, which are created after the localization of excitons in the tail of the alloy potential fluctuation, generated by excitation photons with energy  $I_{ex}$ . The second localized state in the intermediate state consists of A<sup>0</sup>XBMPs formed by the coupling of neutral acceptors and (localized) excitons in the alloy potential fluctuation. By capturing photons associated with the Stokes L<sub>2</sub> line, the electron-hole pairs in some A<sup>0</sup>XBMPs are excited to a state higher in energy than the alloy potential fluctuation; exciton magnetic polarons with higher energy than the excitation photons are then localized in the alloy potential fluctuation, and anti-Stokes PL occurs.

is the percentage of the absorbed photons that create excitons,  $\alpha$  is the absorption coefficient at the excitation frequency  $\nu_{ex}$ ,  $I_{ex}$  is the excitation power,  $x_E$  is the position in the bulk alloy at which an exciton is created,  $p$  is the percentage of created excitons that form excitons localized to the alloy potential fluctuation,  $N_{A_0}$  is the density of neutral acceptors,  $t$  is the time, and  $\tau_L$ ,  $\tau_{A_0X}$ , and  $\tau_{AS}$  are the lifetimes of the LMPs, A<sup>0</sup>XBMPs, and exciton magnetic polarons contributing to the anti-Stokes PL, respectively. In addition,  $C_{L-A_0}$  and  $C_{E-A_0}$  are the capture coefficients of excitons and localized excitons by neutral acceptors contributing to the second localized state, respectively, and  $W$  is the interaction rate of A<sup>0</sup>XBMPs with the radiation due to LMP recombination (the Stokes L<sub>2</sub> line). Here, we have neglected the rate at which LMPs or A<sup>0</sup>XBMPs in the first and second localized states are created by the anti-Stokes PL. We have also assumed that the lifetimes of all exciton magnetic polaron states ( $\tau_L$ ,  $\tau_{A_0X}$ , and  $\tau_{AS}$ ) are constant, that no polaron molecules are formed, and that the effects of particle diffusion are negligible. Furthermore, nonradiative processes are not taken into account. Taking the steady-state solution of the three equations, we obtain the intensity of the anti-Stokes PL ( $I_{AS}$ ) as

$$I_{AS} \propto I_{ex}n_{A_0X}. \quad (4)$$

Therefore in the two-step absorption process occurring in our study,  $I_{AS}$  is proportional to the intensity of the excitation photons and to the density of the A<sup>0</sup>XBMPs. In the low excitation power regime,  $n_{A_0X}$  is not saturated and is then proportional to  $I_{ex}$ . Therefore  $I_{AS}$  is proportional to  $I_{ex}^2$  for excitation powers of less than 3 mW/cm<sup>2</sup>, as shown in Fig. 2. When the excitation power is greater than 3 mW/cm<sup>2</sup>, where  $n_{A_0X}$  is already saturated and reaches a constant value,  $I_{AS}$  is

proportional to  $I_{\text{ex}}$ . Consequently, in mixed-crystal DMS bulk alloys, the necessary conditions for the occurrence of anti-Stokes PL arising from the above two-step absorption process under selective excitation are cooperative transitions between the LMPs via localized excitonic states in the alloy potential fluctuation and  $A^0XBMPs$  via impurity bound states in the vicinity of exciton states. We remark that exciton magnetic polarons are essential for the generation of anti-Stokes PL because the quantum efficiency of the PL rapidly increases when exciton magnetic polarons are formed.<sup>23</sup> Therefore the coefficient  $W$  in Eqs. (2) and (3) might be decreased when the magnetic polaron effect vanishes.

### C. Zeeman shift of Stokes and anti-Stokes photoluminescence with magnetic field

The PL inherently provides significant insight into the magnetic properties because the  $sp-d$  exchange interaction strongly contributes to the energies of localized excitons and exciton magnetic polarons. As the magnetic field increases, the PL peak tends to shift to lower energy because of the giant Zeeman splitting of the valence and conduction bands; however, the disappearance of the exciton magnetic polarons tends to decrease this shift. As shown in Fig. 4, the PL peak positions for  $\sigma^+$  ( $L_2$  line) and  $\sigma^-$  ( $L_1$  line) circularly polarized light, measured in the Faraday configuration under band-to-band excitation, both decrease in energy and become increasingly separated with increasing magnetic field.

The Zeeman splitting is caused by the  $sp-d$  exchange interaction between the spins of the band electrons ( $5s$  or  $5p$  orbitals) and the  $\text{Mn}^{2+}$  spins ( $3d$  orbitals). Phenomenologically, the  $sp-d$  exchange interaction is described by a Heisenberg-type Hamiltonian,

$$H_{sp-d} = \sum_{R_i} J^{sp-d}(r - R_i) S_i \cdot \sigma, \quad (5)$$

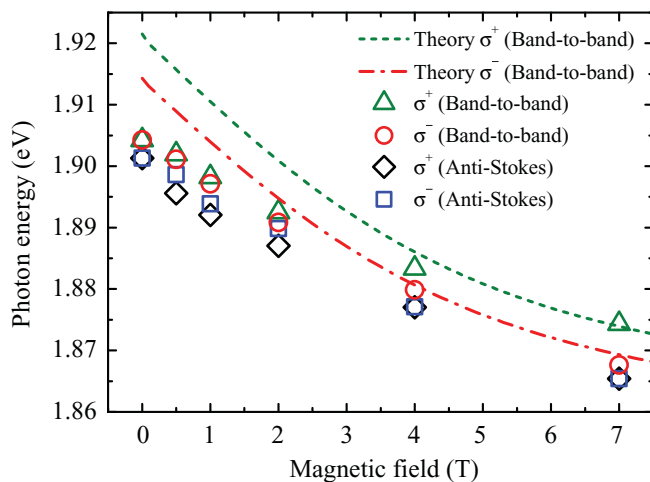


FIG. 4. (Color online) Dependence of PL peak positions for  $\sigma^+$  and  $\sigma^-$  circularly polarized light on magnetic field for both Stokes PL under band-to-band excitation and anti-Stokes PL. The excitation power and temperature were fixed at  $400 \text{ mW/cm}^2$  and  $4.5 \text{ K}$ . The dashed and dashed-dotted lines represent theoretical calculations of the Zeeman shifts of  $\sigma^+$  and  $\sigma^-$  circularly polarized PL under band-to-band excitation, respectively.

where  $S_i$  and  $\sigma$  are the spin operators of the  $\text{Mn}^{2+}$  ion on the lattice site  $R_i$  and of the band electron at  $r$ , respectively.<sup>1</sup> The term  $J^{sp-d}$  is the  $sp-d$  exchange interaction energy, and the summation is over all  $\text{Mn}^{2+}$  ions. Applying the usual mean-field approximation and virtual-crystal approximation to Eq. (5), the Zeeman splitting energy is expressed as  $\pm N_0(\alpha - \beta)x \langle S_z \rangle / 2$  for the  $|\pm 1/2\rangle \rightarrow |\pm 3/2\rangle$  transition and as  $\mp N_0(\alpha + \beta/3)x \langle S_z \rangle / 2$  for the  $|\mp 1/2\rangle \rightarrow |\pm 1/2\rangle$  transition, where  $N_0\alpha$  and  $N_0\beta$  are the  $s$ - and  $p$ - $d$  exchange integrals, respectively; the  $\text{Mn}^{2+}$  ion concentration is denoted by  $x$ , and  $\langle S_z \rangle$  is the average thermal value of  $S_i$ . The notation  $|m_s\rangle \rightarrow |m_j\rangle$  denotes the transition from the  $|m_s\rangle$  electronic state in the conduction band to the  $|m_j\rangle$  electronic state of the valence band. For the excitons of  $\text{Cd}_{1-x}\text{Mn}_x\text{Te}$ , the values of  $N_0\alpha$  and  $N_0\beta$  are  $+0.22 \text{ eV}$  and  $-0.88 \text{ eV}$ , respectively. The exchange interactions between the magnetic moments of the  $\text{Mn}^{2+}$  spins in the  $\text{CdTe}$  matrix are antiferromagnetic for both nearest-neighbor and next-nearest-neighbor exchange.<sup>24</sup> The thermal average value  $\langle S_z \rangle$  of each  $\text{Mn}^{2+}$  spin in  $\text{Cd}_{1-x}\text{Mn}_x\text{Te}$  is given by the following equations<sup>25,26</sup>

$$\langle S_z \rangle = -S_{\text{eff}}(x) B_{5/2} \left\{ \frac{5}{2} \frac{g_{\text{Mn}} \mu_B B}{k [T + T_0(x)]} \right\}, \quad (6)$$

where

$$B_{5/2}(u) = \frac{6}{5} \coth\left(\frac{6}{5}u\right) - \frac{1}{5} \coth\left(\frac{1}{5}u\right), \quad (7)$$

is the Brillouin function for spin  $S = 5/2$ ,  $g_{\text{Mn}}$  is the  $g$  factor of  $\text{Mn}^{2+}$ ,  $\mu_B$  is the Bohr magneton,  $B$  is the magnetic-field strength, and  $T$  is the temperature. The values of  $T_0(x)$  and  $S_{\text{eff}}(x)$  for the  $x = 0.2$  sample are deduced from actual measurements of the Zeeman splitting in bulk alloys to be

$$T_0(x) = \frac{35.37}{1 + 2.752x} x \quad [\text{K}], \quad (8)$$

$$S_{\text{eff}}(x) = \frac{5}{2} [0.265 \exp(-43.34x) + 0.735 \exp(-6.19x)]. \quad (9)$$

Figure 5 shows a comparison of  $xS_{\text{eff}}(x)$  obtained using the empirical equation (9) and using a statistical calculation

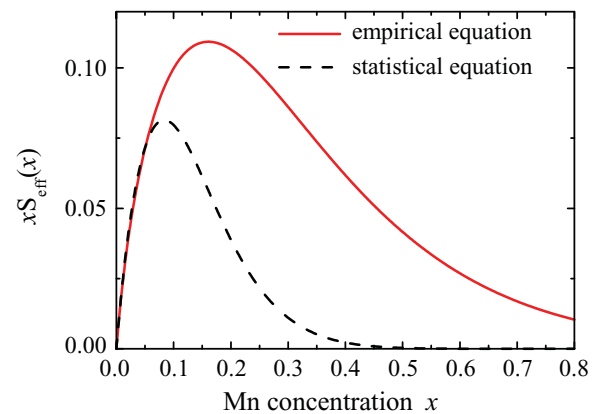


FIG. 5. (Color online) Dependence of  $xS_{\text{eff}}(x)$  on Mn concentration  $x$ , calculated using the empirical equation (9) (solid line) and using a statistical equation (dashed line).

of the bulk magnetization. The statistical calculation takes into consideration the formation of pairs and clusters of nearest-neighbor  $\text{Mn}^{2+}$  spins coupled antiferromagnetically and is expressed as

$$S_{\text{eff}}(x) = \frac{5}{2} \left[ P_1(x) + \frac{P_3^O(x)}{3} + \frac{P_3^C(x)}{15} \right], \quad (10)$$

where  $P_1(x) = (1-x)^{12}$  is the probability of an isolated  $\text{Mn}^{2+}$  cation, and  $P_3^O(x) = 18x^2(1-x)^{23}(7-5x)$  and  $P_3^C(x) = 24x^2(1-x)^{22}$  are the probabilities of  $\text{Mn}^{2+}$  constituting open and closed triplets, respectively.<sup>26</sup> The probability of paired  $\text{Mn}^{2+}$  cations is expressed as  $P_2(x) = 12x(1-x)^{18}$  and does not contribute to the magnetization. As shown in Fig. 5, we find that  $xS_{\text{eff}}(x)$  calculated using the empirical equation is significantly enhanced compared with the statistical calculation for  $x > 0.05$ ; this is due to the large clustering effect at this  $\text{Mn}^{2+}$  concentration.<sup>27</sup>

Under thermal equilibrium, the  $L_2$  line originates from the transition  $|-1/2\rangle \rightarrow |-3/2\rangle$  with  $\sigma^+$  circular polarization, which is shown as the dashed line in Fig. 4. Here, we use Eq. (9) to calculate  $S_{\text{eff}}(x)$ . Using the same procedure, the  $L_1$  line is ascribed to the transition  $|-2, -1/2\rangle \rightarrow |-3/2\rangle$  with  $\sigma^-$  circular polarization,<sup>15</sup> which is represented by the dashed-dotted line in Fig. 4. Here, the notation  $|m_{Jjj}, m_e\rangle$  denotes the  $A^0X$  state derived from two holes coupling  $m_{Jjj}$  with one electron state  $m_e$ . The exchange integrals for the holes in the  $A^0X$  state and the neutral acceptor are assumed to be  $N_0\beta = 0.88$  and  $0.35$  eV, respectively.<sup>15,28</sup> We note that the above-mentioned calculations do not include the effects of exciton magnetic polaron formation. In Fig. 4, the theoretical curve representing the  $L_2$  line has been shifted upwards by 15 meV from 1.906 eV at zero magnetic field by taking into account the localization energy due to the formation of exciton magnetic polarons [see Fig. 1(b)]. This localization energy of 15 meV agrees well with the selective excitation measurements.<sup>23</sup> We have shifted the theoretical curve representing the  $L_1$  line downwards by 7 meV from the  $L_2$  line at zero magnetic field by taking into account the  $A^0X$  binding energy without the magnetic polaron effect.<sup>5</sup> As shown in Fig. 4, the theoretical curve is in good agreement with the experimental data at magnetic fields larger than 4 T, which implies that the magnetic polaron effect exists at fields up to 4 T. These results also indicate that the  $\sigma^+$  circularly polarized PL arises from the LMPs ( $L_2$  line) and that the  $\sigma^-$  PL results from the  $A^0XBMPs$  ( $L_1$  line). The PL due to the recombination of LMPs appears in the vicinity of the PL arising from the recombination of  $A^0XBMPs$ .

The position of the anti-Stokes PL peak exhibits the same behavior with respect to magnetic field. Both  $\sigma^+$  and  $\sigma^-$  circularly polarized PL are observed in the anti-Stokes spectra. Focusing first on the peak position of the  $\sigma^+$  component, it is apparent that the anti-Stokes PL is strongly redshifted with respect to the PL under band-to-band excitation at all values of magnetic field. In contrast, the  $\sigma^-$  anti-Stokes PL peak is observed at only slightly lower energy than the PL peak under band-to-band excitation. The reabsorption effect that takes place inside bulk alloys is the key to elucidating the mechanism of the redshift of anti-Stokes PL. We observed that the peak position of the  $\sigma^+$  component of the anti-Stokes PL does not

depend on the polarization of the excitation light source ( $\sigma^+$  or  $\sigma^-$ ) at low magnetic fields. However, the intensity of the  $\sigma^+$  anti-Stokes PL peak excited by  $\sigma^-$  light is much smaller than that excited by  $\sigma^+$  light at low magnetic fields. This supports our interpretation that the first localized state of the intermediate state is comprised of LMPs, which are involved in the two-step absorption process, by considering the selection rule for the lowest energy transition ( $\sigma^+$ ) from the  $|-3/2\rangle$  electronic state of the valence band to the  $|-1/2\rangle$  electronic state in the conduction band<sup>1</sup>

#### D. Effect of reabsorption of anti-Stokes photoluminescence

For low-energy excitation, the excitation light deeply penetrates into the bulk alloy sample, and anti-Stokes PL is reabsorbed because of the localized exciton or  $A^0X$  lines as it propagates back to the surface. The anti-Stokes PL line shape is modified by reabsorption, which enables us to elucidate the energy of the PL lines inside the sample. Therefore we quantitatively evaluate both the absorption of excitation light and the reabsorption of anti-Stokes PL.

The density of excitons created between sample depths  $x$  and  $x + \Delta x$  in a bulk sample is macroscopically expressed as  $N(x)dx = I(x) - I(x + \Delta x) = -(\partial I/\partial x)dx$ , where  $I(x) = I_{\text{ex}} \exp[-\alpha_{\text{exc}}(\lambda_{\text{ex}})x]$  is the excitation power obtained from the Lambert-Beer law,  $I_{\text{ex}}$  is the intensity of the incident light (the number of contributory photons per  $\text{cm}^2$  per second), and  $\alpha_{\text{exc}}(\lambda_{\text{ex}})$  is the absorption coefficient of the excitation light with wavelength  $\lambda_{\text{ex}}$  in the presence of excitons. The PL intensity with no reabsorption effect, namely the case of band-to-band excitation, is written as

$$I_B(\lambda) = \eta_B \int_0^\infty N(x)dx = \eta_B I_{\text{ex}} \alpha_{\text{exc}}(\lambda_{\text{ex}}) \times \int_0^\infty \exp[-\alpha_{\text{exc}}(\lambda_{\text{ex}})x]dx = \eta_B I_{\text{ex}}, \quad (11)$$

where  $\eta_B$  is the radiative efficiency under band-to-band excitation. The intensity of the anti-Stokes PL taking into account the reabsorption effect can then be expressed as

$$I_{\text{AS}}(\lambda) = \eta_{\text{AS}} I_{\text{ex}} \alpha_{\text{exc}}(\lambda_{\text{ex}}) \int_0^\infty \exp\{-[\alpha_{\text{exc}}(\lambda_{\text{ex}}) + \alpha(\lambda)]x\}dx = \frac{\eta_{\text{AS}} I_{\text{ex}} \alpha_{\text{exc}}(\lambda_{\text{ex}})}{\alpha_{\text{exc}}(\lambda_{\text{ex}}) + \alpha(\lambda)}, \quad (12)$$

where  $\eta_{\text{AS}}$  is the radiative efficiency of the anti-Stokes PL, and  $\alpha(\lambda)$  is the one-photon absorption coefficients at anti-Stokes PL wavelengths. If we assume that the thickness of the bulk alloy is much greater than  $\alpha^{-1}(\lambda)$  and  $\alpha_{\text{exc}}^{-1}(\lambda_{\text{ex}})$ , then

$$\frac{I_B}{I_{\text{AS}}}(\lambda) = \frac{\eta_B}{\eta_{\text{AS}}} \frac{\alpha_{\text{exc}}(\lambda_{\text{ex}}) + \alpha(\lambda)}{\alpha_{\text{exc}}(\lambda_{\text{ex}})}. \quad (13)$$

In the case of selective excitation where  $\lambda \approx \lambda_{\text{ex}}$ , the absorption coefficient of the excitation light is approximately equal to that of the PL at the excitation wavelength. Thus we can assume that  $\alpha(\lambda \approx \lambda_{\text{ex}}) \approx \alpha_{\text{exc}}(\lambda_{\text{ex}})$ , which leads to the expression  $I_B/I_{\text{AS}}(\lambda \approx \lambda_{\text{ex}}) \approx 2\eta_B/\eta_{\text{AS}}$ . We then obtain

$$\frac{\alpha(\lambda)}{\alpha_{\text{exc}}(\lambda_{\text{ex}})} = 2 \frac{I_B}{I_{\text{AS}}}(\lambda) \cdot \frac{I_{\text{AS}}}{I_B}(\lambda_{\text{ex}}) - 1, \quad (14)$$

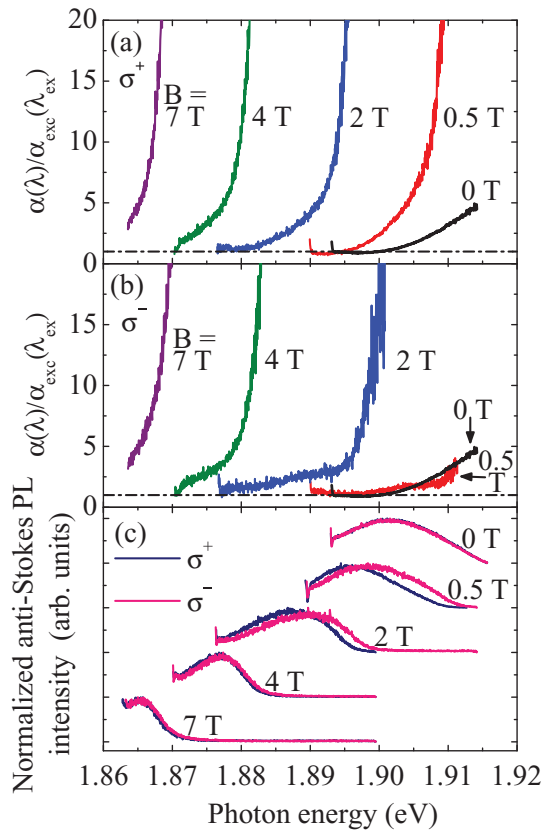


FIG. 6. (Color online) Ratio of the absorption coefficients  $\alpha(\lambda)$  and  $\alpha_{\text{exc}}(\lambda_{\text{exc}})$  for selective excitation under various magnetic fields for (a) the  $\sigma^+$  component and (b) the  $\sigma^-$  component of the anti-Stokes PL. The dashed-dotted line indicates  $\alpha(\lambda) = \alpha_{\text{exc}}(\lambda_{\text{exc}})$ . (c) Evolution of the corresponding anti-Stokes PL spectra with magnetic field. The intensity has been normalized by the peak intensity. The excitation power was fixed at  $400 \text{ mW/cm}^2$  and the temperature was fixed at  $4.5 \text{ K}$ .

which suggests that the ratio  $I_B/I_{\text{AS}}(\lambda)$  is proportional to  $\alpha(\lambda)$ . Figures 6(a) and 6(b) show the evolution of  $\alpha(\lambda)/\alpha_{\text{exc}}(\lambda_{\text{exc}})$  with photon energy at various magnetic fields for both the  $\sigma^+$  and  $\sigma^-$  anti-Stokes PL components, using a  $\sigma^+$  circularly polarized excitation light source.  $\alpha(\lambda)$  for the  $\sigma^+$  and  $\sigma^-$  components represents the shift of the localized exciton absorption edge and the  $A^0X$  absorption edge, respectively. Both would be modified by the formation of other magnetic polarons, which contribute to the two-step processes where the anti-Stokes PL propagates. Therefore the localized exciton and  $A^0X$  absorption edges in the absence of magnetic polaron effects should appear at  $7 \text{ T}$  in Figs. 6(a) and 6(b), respectively. We note that the shape of the  $\alpha(\lambda)/\alpha_{\text{exc}}(\lambda_{\text{exc}})$  curve is meaningful when considering the effect of reabsorption. The ratio  $\alpha(\lambda)/\alpha_{\text{exc}}(\lambda_{\text{exc}})$  is larger than 1 [indicated by the dashed-dotted line in Figs. 6(a) and 6(b)], implying that  $\alpha_{\text{exc}}(\lambda_{\text{exc}}) \approx \alpha(\lambda_{\text{exc}}) \leq \alpha(\lambda)$ , because the density of energy levels of the localized exciton states gradually decreases as the excitation energy is decreased below the energy of the PL peak position [see the inset of Fig. 1(d)]. We also measured  $\alpha(\lambda)/\alpha_{\text{exc}}(\lambda_{\text{exc}})$  while varying the excitation energy and intensity at zero magnetic field; no significant changes in the shape of the curve were observed. The corresponding normalized anti-Stokes PL

spectra are shown in Fig. 6(c). No differences in the spectra of the  $\sigma^+$  and  $\sigma^-$  anti-Stokes PL are observed at zero magnetic field, which is due to the degeneracy of the LMP and  $A^0XBMP$  states.<sup>15</sup>

We now focus our discussion on the high-energy side of the anti-Stokes PL line, where reabsorption is prominent. The reabsorption coefficient of the  $\sigma^+$  anti-Stokes PL line rapidly increases with increasing incident photon energy. In low magnetic fields ( $B < 4 \text{ T}$ ), the density of states of the  $\sigma^+$  anti-Stokes PL lines is reduced in energy by the formation of LMPs inside the sample, which implies that the corresponding spectral line is located at a slightly lower energy than the localized exciton line. Therefore the higher-energy side of the  $\sigma^+$  anti-Stokes PL line is reabsorbed via the localized exciton absorption process as it propagates back to the surface. For magnetic fields  $B > 4 \text{ T}$ , the energy difference between the localized exciton absorption line and the  $\sigma^+$  anti-Stokes PL line decreases because the magnetic polaron effect disappears. Therefore a greater degree of reabsorption occurs on the  $\sigma^+$  anti-Stokes PL. Furthermore, the width of the  $\sigma^+$  anti-Stokes PL decreases with increasing magnetic field due to both a shift of the absorption coefficient edge and extinction of the LMPs, as shown in Fig. 6(c). This increasing reabsorption effect provides a good explanation for the  $\sigma^+$  anti-Stokes PL peak position, which is found at much lower energy than that of the PL peak under band-to-band excitation (Fig. 4). The  $\sigma^-$  anti-Stokes PL component follows the same tendency as the  $\sigma^+$  component in magnetic fields  $B > 4 \text{ T}$ , where the magnetic polarons no longer exist. In contrast, at low magnetic fields ( $B < 2 \text{ T}$ ) the absorption coefficient remains almost constant in the  $\sigma^-$  anti-Stokes PL energy regime, which implies that the  $\sigma^-$  anti-Stokes PL spectra are not modified by the reabsorption effect.

We assume the low degree of reabsorption in the  $\sigma^-$  anti-Stokes PL to be likely caused by the relatively larger energy shift of the anti-Stokes PL line compared with that of the  $A^0X$  absorption line. This is ascribed to photoinduced localized  $\text{Mn}^{2+}$  spin ordering around  $A^0XBMPs$ , which competes with  $\text{Mn}^{2+}$  antiferromagnetic interactions. In the following discussion, we explain how a parallel orientation of local  $\text{Mn}^{2+}$  spins is caused by the  $A^0XBMPs$ . The interactions of the  $\text{Mn}^{2+}$  spins around  $A^0XBMPs$  is the dominant cause of local  $\text{Mn}^{2+}$  spin alignment via optical pumping, because with the hydrogen model, the wave function of the holes in the  $A^0X$  state is greatly expanded in comparison to that in a neutral acceptor.<sup>5</sup> We assume the strength of the photoinduced localized  $\text{Mn}^{2+}$  spin ordering depends on the spin configurations of the two holes in  $A^0X$ . The  $A^0X$  state is composed of one electron and two holes, which play a dominant role in the formation of magnetic polarons because the absolute value of the  $p$ - $d$  exchange constant is larger than that of the  $s$ - $d$  exchange constant. As described in the previous section, in terms of the  $j$ - $j$  coupling scheme, the total angular momentum of the two holes in the lowest energy  $A^0X$  state is large ( $J_{jj} = 2$ ). As a consequence, the parallel orientation of local  $\text{Mn}^{2+}$  spins due to the  $A^0XBMPs$  would be dominant inside the sample at low magnetic fields. The  $A^0XBMPs$  exist only in external magnetic fields up to  $3 \text{ T}$ ,<sup>13</sup> for which a low degree of reabsorption is observed in the  $\sigma^-$  anti-Stokes PL. This also supports our experimental results in Fig. 4, which

indicate that the  $A^0XBMPs$  vanish at magnetic fields higher than 4 T. The parallel orientation of local  $Mn^{2+}$  spins might be considerably small to observe by using standard absorption measurement of thin samples. However, this effect can be observed using reabsorption measurements under selective excitation, because the excitation light penetrates deep into the bulk alloy sample and anti-Stokes PL is reabsorbed as it propagates back to the surface. Therefore the interaction length of the excitation light with excitonic matter should be enhanced using this method. To probe the effect of the parallel orientation of local  $Mn^{2+}$  spins due to the  $A^0XBMPs$  without suppressing the exciton magnetic polarons, moderate magnetic-field strengths ( $\sim 0.5$  T) are suitable. We note that the reabsorption shift does not depend on the excitation density, which is attributed to saturation of the available acceptors. We also note that a photoinduced magnetic-phase transition would be generated by long-range ferromagnetic ordering induced by percolation of magnetic polarons<sup>9</sup> or long-range ferromagnetic interactions between photogenerated holes. This scenario would become possible when the hole density considerably exceeds the impurity density.<sup>29</sup> However, we are unable to demonstrate such situation in our current study. This is because the direction of the magnetic moments of the LMPs is opposite to that of the  $A^0XBMPs$ ,<sup>15</sup> which prevents long-range ferromagnetic ordering under high-density excitation.

### E. Other remarks concerning bound magnetic polaron effects

It has been reported that the  $A^0X$  state diminishes in an external magnetic field due to ionization of its loosely bound electron,<sup>13,15</sup> this indicates that the anti-Stokes PL should be suppressed due to the attenuation of the second localized state in the intermediate state, as well as the reabsorption effect and the disappearance of the magnetic polarons. It is worth focusing on the “photon recycling” process and its influence on the intensity of the anti-Stokes PL. Figure 7 shows the dependence of the peak intensities of the  $\sigma^+$  circularly polarized anti-Stokes and Stokes PL, using a  $\sigma^+$  circularly polarized excitation light source. With increasing magnetic field, the intensity of the anti-Stokes PL abruptly decreases, whereas the Stokes PL intensity remains almost constant up

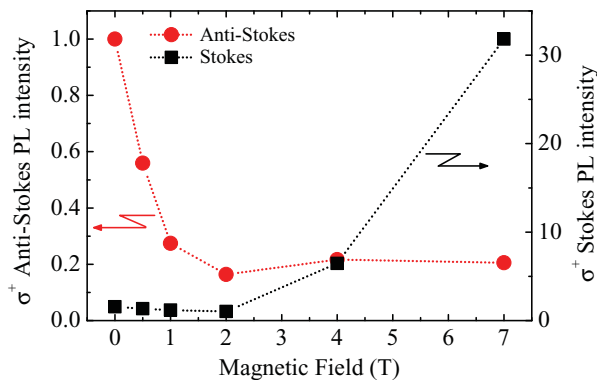


FIG. 7. (Color online) Dependence of peak intensity on magnetic field for the  $\sigma^+$  circularly polarized anti-Stokes and Stokes PL. The intensity has been normalized to that at zero magnetic field for both the Stokes and the anti-Stokes PL. The excitation power and temperature were fixed at  $400 \text{ mW/cm}^2$  and  $4.5 \text{ K}$ .

to 2 T despite the occurrence of intensity amplification due to directional dipole radiation.<sup>15</sup> This indicates that the “photon recycling” process should take place at magnetic fields up to at least 2 T, due to the existence of  $A^0XBMPs$  in the intermediate state. Therefore the abrupt reduction of the anti-Stokes PL intensity is due to the disappearance of the intermediate state, as well as the reabsorption effect and the extinction of the magnetic polarons. This field of 2 T is smaller than that obtained in Fig. 4 and smaller than the field that was previously reported to be necessary<sup>13</sup> to extinguish the  $A^0XBMPs$ . This implies that, despite the existence of  $A^0XBMPs$  at fields higher than 2 T, their density is insufficient to induce significant “photon recycling.” The residual intensity of the anti-Stokes PL at higher fields might be caused by another minor process, for example, the presence of localized excitons as both the first and second localized states.

The  $A^0XBMPs$  play two important roles in  $Cd_{0.8}Mn_{0.2}Te$ . The first involves the intermediate state in the two-step absorption process that contributes to the appearance of anti-Stokes PL, and the second involves the generation of photoinduced localized  $Mn^{2+}$  spins ordering inside bulk alloy samples. In this study we have assumed that the two phenomena take place independently of each other.

We also remark on the neutral acceptor ground state, which might be modulated in energy by the formation of BMPs. The neutral acceptor ground state is stable due to the magnetic polaron effect (here, we refer to this state as “ $A^0BMP$ ”) at low temperature.<sup>30</sup>  $Mn^{2+}$  spins around an  $A^0$  neutral acceptor will be aligned to a greater extent after dissociation of the  $A^0XBMP$ . After coupling with a photoexcited exciton, an  $A^0X$  state is formed and soon becomes an  $A^0XBMP$  state via the magnetic polaron effect. When  $Mn^{2+}$  spins inside the  $A^0X$  Bohr radius become better aligned, radiative recombination then occurs leaving the  $A^0BMP$  state, which is more stable than the inherent  $A^0$  neutral acceptor state. Therefore it should be possible to induce modulation of the energy of the  $A^0$  neutral acceptor ground state by selective optical pumping; further investigations are necessary.

The combination of anti-Stokes PL with BMPs is advantageous from the point of view of practical applications compared with the potential of nonmagnetic mixed crystals,<sup>3</sup> because the magnetic spins can be controlled by the formation of magnetic polarons. The anti-Stokes PL process might become more effective if improvements could be made to the “recycling” of photons in the two-step absorption process. We expect that this study will contribute to the development of novel technology based on photoinduced magnetization for applications that take advantage of optical pumping, such as self-magnetic optical cooling.

## IV. CONCLUSIONS

We have observed anti-Stokes PL in bulk alloys of the diluted magnetic semiconductor  $Cd_{0.8}Mn_{0.2}Te$  under selective excitation. The anti-Stokes PL peak results from a two-step absorption process via cooperative excitations involving the  $A^0XBMPs$  and LMPs. We propose a model in which certain photoexcited excitons bind to the acceptors to form  $A^0XBMPs$ ; a proportion of the energy of the Stokes PL that

arises from recombination of electron-hole pairs consisting of LMPs is then transferred to the  $A^0XBMPs$ , resulting in excitation to energies above the alloy potential fluctuation. We have also demonstrated that  $\sigma^+$  circularly polarized PL due to the recombination of LMPs appears in the vicinity of  $\sigma^-$  circularly polarized PL arising from the recombination of  $A^0XBMPs$ . Due to reabsorption effects, both anti-Stokes PL lines appear at lower energy than the PL under band-to-band excitation. At low magnetic fields, we propose that the degree of reabsorption of the  $\sigma^-$  circularly polarized anti-Stokes PL

is low; this is attributed to the generation of photoinduced localized  $Mn^{2+}$  spin ordering within  $A^0XBMPs$ .

#### ACKNOWLEDGMENTS

This study was supported by the Program for Improvement of Research Environment for Young Researchers from the Special Coordination Funds for Promoting Science and Technology (SCF), commissioned by the Ministry of Education, Culture, Sports, Science and Technology (MEXT) of Japan.

- 
- <sup>1</sup>J. K. Furdyna, *J. Appl. Phys.* **64**, R29 (1988).  
<sup>2</sup>O. Goede and W. Heimbrod, *Phys. Status Solidi B* **146**, 11 (1988).  
<sup>3</sup>S. Permogorov, A. Reznitsky, S. Verbin, G. O. Müller, P. Flögel, and M. Nikiforova, *Phys. Status Solidi B* **113**, 589 (1982).  
<sup>4</sup>J. A. Gaj, R. R. Gałazka, and M. Nawrocki, *Solid State Commun.* **25**, 193 (1978).  
<sup>5</sup>A. Golnik, J. Ginter, and J. A. Gaj, *J. Phys. C* **16**, 6073 (1983).  
<sup>6</sup>H. Krenn, W. Zawadzki, and G. Bauer, *Phys. Rev. Lett.* **55**, 1510 (1985).  
<sup>7</sup>H. Ohno, *Science* **281**, 951 (1998).  
<sup>8</sup>A. C. Durst, R. N. Bhatt, and P. A. Wolff, *Phys. Rev. B* **65**, 235205 (2002).  
<sup>9</sup>A. Kaminski and S. Das Sarma, *Phys. Rev. Lett.* **88**, 247202 (2002).  
<sup>10</sup>T. Dietl, H. Ohno, F. Matsukura, J. Cibert, and D. Ferrand, *Science* **287**, 1019 (2000).  
<sup>11</sup>A. Haury, A. Wasiela, A. Arnoult, J. Cibert, S. Tatarenko, T. Dietl, and Y. M. d'Aubigné, *Phys. Rev. Lett.* **79**, 511 (1997).  
<sup>12</sup>A. Lipińska, C. Simserides, K. N. Trohidou, M. Goryca, P. Kossacki, A. Majhofer, and T. Dietl, *Phys. Rev. B* **79**, 235322 (2009).  
<sup>13</sup>D. Heiman, P. Becla, R. Kershaw, D. Ridgley, K. Dwight, A. Wold, and R. R. Galazka, *Phys. Rev. B* **34**, 3961 (1986).  
<sup>14</sup>J. I. Jang, S. Mani, J. B. Ketterson, and H. Y. Park, *Phys. Rev. B* **77**, 235211 (2008).  
<sup>15</sup>T. Okada and T. Itoh, *J. Phys.: Condens. Matter* **19**, 186210 (2007).  
<sup>16</sup>R. Hellmann, A. Euteneuer, S. G. Hense, J. Feldmann, P. Thomas, E. O. Göbel, D. R. Yakovlev, A. Waag, and G. Landwehr, *Phys. Rev. B* **51**, 18053 (1995).  
<sup>17</sup>V. Y. Ivanov, Y. G. Semenov, M. Surma, and M. Godlewski, *Phys. Rev. B* **54**, 4696 (1996).  
<sup>18</sup>W. Heimbrod, M. Happ, and F. Henneberger, *Phys. Rev. B* **60**, R16326 (1999).  
<sup>19</sup>E. Finkeiß, M. Potemski, P. Wyder, L. Viña, and G. Weimann, *Appl. Phys. Lett.* **75**, 1258 (1999).  
<sup>20</sup>R. R. Galazka, S. Nagata, and P. H. Keesom, *Phys. Rev. B* **22**, 3344 (1980).  
<sup>21</sup>G. Mackh, W. Ossau, D. R. Yakovlev, A. Waag, G. Landwehr, R. Hellmann, and E. O. Göbel, *Phys. Rev. B* **49**, 10248 (1994).  
<sup>22</sup>F. A. J. M. Driessen, *Appl. Phys. Lett.* **67**, 2813 (1995).  
<sup>23</sup>T. Itoh and E. Komatsu, *J. Lumin.* **38**, 266 (1987).  
<sup>24</sup>B. E. Larson, K. C. Hass, H. Ehrenreich, and A. E. Carlsson, *Phys. Rev. B* **37**, 4137 (1988).  
<sup>25</sup>J. A. Gaj, W. Grieshaber, C. Bodin-Deshayes, J. Cibert, G. Feuillet, Y. Merle d'Aubigné, and A. Wasiela, *Phys. Rev. B* **50**, 5512 (1994).  
<sup>26</sup>W. Grieshaber, A. Haury, J. Cibert, Y. M. d'Aubigné, A. Wasiela, and J. A. Gaj, *Phys. Rev. B* **53**, 4891 (1996).  
<sup>27</sup>J. M. Fatah, T. Piorek, P. Harrison, T. Stirner, and W. E. Hagston, *Phys. Rev. B* **49**, 10341 (1994).  
<sup>28</sup>A. K. Bhattacharjee, *Phys. Rev. B* **58**, 15660 (1998).  
<sup>29</sup>D. J. Priour Jr. and S. Das Sarma, *Phys. Rev. Lett.* **97**, 127201 (2006).  
<sup>30</sup>T. H. Nhung, R. Planel, C. Benoit à la Guillaume, and A. K. Bhattacharjee, *Phys. Rev. B* **31**, 2388 (1985).